

Exactly solvable spin-glass models with ferromagnetic couplings: the spherical multi- p -spin model in a self-induced field

Andrea Crisanti^{1,2}, Luca Leuzzi^{1,3}

¹ *Dipartimento di Fisica, Università di Roma "La Sapienza", P.le Aldo Moro 5, 00185 Roma, Italy*

² *CNR-ISC, Via dei Taurini 19, 00185 Rome, Italy*

³ *CNR-IPCF, UOS Roma, P.le Aldo Moro 5, 00185 Rome, Italy*

Abstract

We report some results on the quenched disordered Spherical multi- p -Spin Model in presence of ferromagnetic couplings. In particular, we present the phase diagrams of some representative cases that schematically describe, in the mean-field approximation, the behavior of most known transitions in glassy materials, including dynamic arrest in super-cooled liquids, amorphous-amorphous transitions and spin-glass transitions. A simplified notation is introduced in order to compute systems properties in terms of an effective, self-induced, field encoding the whole ferromagnetic information.

1. Introduction

In the very extended framework of complex systems, spin glasses have become the source of ideas and techniques now representing a valuable theoretical background in diverse fields, with applications far beyond the physics of amorphous materials (both magnetic and structural). These systems are characterized by a strong dependence from the details, so strong that their behavior cannot be rebuilt starting from the analysis of a single cell constituent. Their analysis cannot be carried out without considering the collective behavior of the whole system. One of the common features is the occurrence of a large number of stable and metastable states or, in other words, a large choice in the possible realizations of the system. This goes along with a rather slow evolution through many, detail-dependent intermediate states, looking for a global equilibrium state (or optimal solution). Mean-field models have largely helped in comprehending many of the mechanisms yielding such complicated structure and also have produced new theories or combined among each other old concepts pertaining to other fields such as, e.g., the spontaneous breaking of the replica symmetry and the ultrametric structure of states. Among mean-field models,

spherical models - i.e., continuous dynamic variables with a global constraint [1]- are analytically solvable even in the most complicated cases.

Multi- p -spin spherical models have been shown to yield low temperature amorphous phases that, depending on the dominant interaction terms, can both be described by discontinuous and continuous Replica Symmetry Breaking (RSB) Ansätze. In particular, (i) one step replica symmetry breaking (1RSB) phases were studied, because of their relevance for the structural glass transition [2, 3, 4, 5], (ii) two step RSB phases [6, 7] are found that are thermodynamically stable and whose dynamics models secondary relaxation in glass-forming liquids (see, e.g., [8] and for a thorough overview [9] and references therein) and study the singularities in the phase diagrams predicted by the mode coupling theory [10, 11, 12], (iii) the Full RSB phase represents spin-glasses in the proper sense and, more generally, the frozen phase in random manifold problems [13, 14, 15, 16, 17]. The possibility of the existence of Full RSB in spherical models was first pointed out by Nieuwenhuizen [18] on the basis of the similarity between the replica free energy multi-spin models and the relevant part of the free energy of the Sherrington-Kirkpatrick model. In Refs. [19, 20] thermodynamic stable Full RSB phases have been actually computed and analyzed. Spherical models, thus, also provide a much simpler realization of this Ansatz than in the spin-glass mean-field prototype model, i.e., the Sherrington-Kirkpatrick model [21].

Further including ordered interaction terms representing attractive ferromagnetic couplings between spins, one can use these models to study diverse problems, such as disordered systems along the Nishimori line [22, 23], or the states following problem [24, 25, 26], else the random pinning with a system at a very high temperature, or in presence of external random constraints, as, e.g., in porous media [27, 28, 29]. Spherical models with competing disordered and ordered non-linear couplings also describe mode-locking laser models, where spherical spins are used to represent both real and imaginary parts of the complex amplitude of photonic modes [30, 31, 32]. In particular, they can be used to address the problem of random lasers [33, 34], whose statistical mechanics description involves interactions between modes that are both non-linear and partially quenched disordered [35, 36]. In the latter case, we notice that the global spherical constraint on continuous variables is not implemented to approximate discrete spin variables or ease the computation of the properties of continuous spins of fixed magnitude (like XY or Heisenberg spins), but it represents the total amount of energy that an external pumping laser beam forces into the random laser to activate its modes.

We will show in this work that adding purely ferromagnetic terms to the quenched disordered ones (a particular case of which is to have quenched disorder with non-zero average) can be simply encoded into adding an effective field to the purely disordered system. The paper is organized as follow: in Sec. 2 we introduce the model and present a formal solution in the framework of Parisi Replica Symmetry Breaking Theory for the general case; in Sec. 3 we specialize the analysis to the $s + p$ case in an uniform external field; in Secs. 4 and 5 we study the behavior in presence of ferromagnetic couplings of two qualitatively

different models both yielding RS and 1RSB phases: the $3 + 4$ and the $2 + 3$ models; in Sec. 6 we consider Replica Symmetry Breaking phases with continuous breakings and in Sec. 7 we show an explicit case in which these phases appear, even in presence of competing ferromagnetic interactions. Eventually, in Sec. 8 we show the temperature vs. degree of order phase diagrams for the $2 + p$ and the $3 + 4$ models, where the degree or order is yielded by a combination of ferromagnetic interaction magnitudes. A word of caution. When the phase is described by a step-like order parameter function, as the 1RSB phase, or it possesses a step-like part, the transition between different phases can differ if one considers the static or dynamic properties of the model [2, 3, 37, 38]. When they are distinct one speaks of the static and dynamic transitions. In the main text we shall consider only the static transitions. The changes associated with the dynamic transition will be briefly discussed in Appendix B.

2. The Model

We consider the general model system described by the spin-Hamiltonian

$$\mathcal{H} = - \sum_{p \geq 2} \sum_{i_1 < \dots < i_p} J_{i_1 \dots i_p}^{(p)} \sigma_{i_1} \dots \sigma_{i_p} - \sum_{k \geq 1} \frac{J_0^{(k)}}{N^{k-1}} \sum_{i_1 < \dots < i_k} \sigma_{i_1} \dots \sigma_{i_k} \quad (1)$$

with both quenched, independently distributed, Gaussian p -spin interactions of zero mean and variance

$$\left[\left(J_{i_1 \dots i_p}^{(p)} \right)^2 \right] = \frac{p! J_p^2}{2N^{p-1}}, \quad (2)$$

and uniform k -spin interactions $J_0^{(k)}$, with the $k = 1$ term representing the interaction with an external uniform field. The scaling of the interaction with the system size N ensures the correct thermodynamic limit $N \rightarrow \infty$. The spins are real continuous variables ranging from $-\infty$ to $+\infty$, subjected to the global spherical constraint $\sum_i \sigma_i^2 = N$ that limits the fluctuations and makes the partition function well defined. The dynamics of the case with a single $p > 2$ term and $k = 2$ was treated in Ref. [39].

The model can also be seen as a spherical multiple-spin interaction Spin Glass model with random couplings of *non-zero* average. The formulation (1) is, however, more general since it gives more freedom in choosing the interactions in the disordered and ordered part of the Hamiltonian. To stress this point we have deliberately used different indexes, namely p and k , for the disordered and ordered interactions.

In the present study we shall consider the sub-class of models where only two terms, one with s and one with $p > s$ interactions, are retained in the disordered part. These models have been called spherical $s + p$ models [19, 20, 40, 41, 6]. The hallmark of these models are different phase diagrams depending on the values of s and p . Representative values of s and p will be discussed when needed.

2.1. The partition sum and replicas

The static properties of the model are obtained from the free energy computed for fixed interactions and then averaged over the disorder. This *quenched* free energy can be computed using the *replica trick*: one first computes the *annealed* free energy density $\Phi(n)$ of n non-interacting identical *replicas* of the system by rising the partition sum $Z = \text{Tr}_\sigma e^{-\beta \mathcal{H}}$ to the n 'th power and averaging it over the disorder:

$$\Phi(n) = - \lim_{N \rightarrow \infty} \frac{1}{\beta N n} \ln [Z^n]. \quad (3)$$

The *quenched* free energy density Φ is then obtained from the continuation of $\Phi(n)$ to non-integer values of n down to $n = 0$:

$$\Phi = - \lim_{N \rightarrow \infty} \lim_{n \rightarrow 0} \frac{1}{\beta N n} ([Z^n] - 1) = \lim_{n \rightarrow 0} \Phi(n). \quad (4)$$

In the last equality we assumed that the thermodynamic limit $N \rightarrow \infty$ and the replica limit $n \rightarrow 0$ can be exchanged. The calculation of $[Z^n]$ is rather standard, so we report the main steps, just in order to introduce our notation. The interested reader can find more details in Refs. [42, 5]. By introducing the collective variables

$$q_{ab} = \frac{1}{N} \sum_i \sigma_i^a \sigma_i^b, \quad m_a = \frac{1}{N} \sum_i \sigma_i^a \quad (5)$$

where $a, b = 1, \dots, n$ are *replica indexes*, with $q_{aa} = 1$ from the spherical constraint, the leading contribution to $[Z^n]$ for $N \rightarrow \infty$ can be written as

$$[Z^n] \sim \int \mathcal{D}[q, \lambda, m, y] e^{-NG[q, \lambda, m, y]}, \quad N \rightarrow \infty \quad (6)$$

where $\mathcal{D}[q, \lambda, m, y] \propto \prod_{a < b} dq_{ab} \prod_{a \leq b} \lambda_{ab} \prod_a dm_a \prod_a dy_a$ denotes integrations over all (free) variables and

$$\begin{aligned} G[q, \lambda, m, y] = & -\frac{1}{2} \sum_{ab} g(q_{ab}) - \sum_a \kappa(m_a) + \frac{1}{2} \sum_{ab} \lambda_{ab} q_{ab} + \sum_a y_a m_a \\ & + \frac{1}{2} \ln \text{Det}(-\lambda) + \frac{1}{2} \sum_{ab} y_a (\lambda^{-1})_{ab} y_b. \end{aligned} \quad (7)$$

We have introduced the short-hand notation:

$$g(q) = \sum_{p \geq 2} \frac{\mu_p}{p} q^p, \quad \mu_p = \frac{p}{2} \beta^2 J_p^2 \quad (8)$$

$$\kappa(m) = \sum_{k \geq 1} b_k m^k, \quad b_p = \frac{\beta}{k!} J_0^{(k)} \quad (9)$$

In the thermodynamic limit $N \rightarrow \infty$ the integrals can be evaluated using the saddle-point approximation, leading to

$$\beta\Phi = \lim_{n \rightarrow 0} \frac{1}{n} \text{Extr } G[q, m] \quad (10)$$

with

$$G[q, m] = -\frac{1}{2} \sum_{ab} g(q_{ab}) - \sum_a \kappa(m_a) - \frac{1}{2} \text{Tr} \ln(q_{ab} - m_a m_b) \quad (11)$$

The functional $G[q, m]$ must be evaluated at its stationary point that, as $n \rightarrow 0$, gives the maximum with respect to variations of q_{ab} and the minimum for variations in m_a . The variables λ_{ab} and y_a have been eliminated via the stationary point equations. In the expression (10) we have not included a constant term $\beta\Phi_0$ that comes from neglected $O(N)$ terms. This fixes the zero temperature value of energy and entropy, but it is not relevant for the study of the phase diagram.

Since we are interested into the limit $n \rightarrow 0$, the expression of $G[q, m]$ can be simplified further by noticing that

$$\text{Tr} \ln(q_{ab} - m_a m_b) = \text{Tr} \ln q - \sum_{ab} m_a (q^{-1})_{ab} m_b + O(n^2) \quad (12)$$

so we arrive at the final expression

$$G[q, m] = -\frac{1}{2} \sum_{ab} g(q_{ab}) - \sum_a \kappa(m_a) - \frac{1}{2} \text{Tr} \ln q + \frac{1}{2} \sum_{ab} m_a (q^{-1})_{ab} m_b + O(n^2). \quad (13)$$

By imposing stationarity of $G[q, m]$ with respect to variations with respect to m_a and q_{ab} ($a \neq b$) we obtain the stationary point equations:

$$b(m_a) = \sum_b (q^{-1})_{ab} m_b \quad (14)$$

$$\Lambda(q_{ab}) + (q^{-1})_{ab} - \sum_c (q^{-1})_{ac} m_c \sum_c (q^{-1})_{bc} m_c = 0, \quad a \neq b \quad (15)$$

$$\Lambda(q) \equiv \frac{dg(q)}{dq} \quad ; \quad b(m) \equiv \frac{d\kappa(m)}{dm}. \quad (16)$$

To solve these equations we observe that eq. (14) can be inverted to give

$$m_a = \sum_b q_{ab} b(m_b). \quad (17)$$

If we retain only the $k = 1$ term in $\kappa(m)$, then $b(m) = b_1$. The equation becomes $m_a = b_1 \sum_b q_{ab}$ and m_a does not depend on the replica index a . This remains true in the general case because there are no explicit replica symmetry

breaking fields. The stationary point equation for the magnetization $m_a \equiv m$ then becomes

$$m = b(m) \sum_{b=1}^n q_{ab} \quad \forall a = 1, \dots, n \quad (18)$$

and the stationary point equation for q_{ab}

$$\Lambda(q_{ab}) + (q^{-1})_{ab} + b(m)^2 = 0 \quad a \neq b. \quad (19)$$

Note that if we consider the value of $b(m)$ as given, that is $b(m) = b$, Eq. (19) reduces to that of the model in an external uniform constant field $h = Tb$. This is a rather important technical point because we can split-up the resolution of the stationary point equation into two steps. First we solve eq. (19) assuming $b(m) = b$ as fixed. Next we look for m solution of eq. (18) such that $b(m) = b$. In the following we will generically refer to b as “field”.

2.2. Parisi Parametrization: Replica Symmetry Breaking

To solve the self-consistent stationary point equation (19) an assumption on the structure of the overlap matrix q_{ab} must be done. As the n replicas of the real system are identical, one may reasonably assume that the solution should be symmetric under the exchange of any pair of replicas. In the high temperature (or field) case this holds true, and the solution is of the form

$$q_{ab} = \delta_{ab} + (1 - \delta_{ab}) q_0. \quad (20)$$

This form of q_{ab} is known as the Replica Symmetric (RS) solution.

As the temperature (and field) decrease the symmetry under replica exchange is spontaneously broken, and the overlap matrix becomes a non-trivial function of the replica indexes. In this regime the RS assumption is not valid and a more complex structure arises. Following the parameterization introduced by Parisi [43, 44], the overlap matrix q_{ab} for R steps of replica permutation symmetry breaking – called RSB solution – is divided along the diagonal into successive blocks of decreasing size p_u , with $p_0 = n$ and $p_{R+1} = 1$, and elements given by:

$$q_{ab} = q_{a \cap b} = q_u, \quad u = 0, \dots, R+1 \quad (21)$$

with $1 = q_{R+1} \geq q_R \geq \dots \geq q_1 > q_0$. In this notation $u = a \cap b$ denotes the overlap between the replicas a and b , and means that a and b belong to the same box of size p_u but to two distinct boxes of size $p_{u+1} < p_u$.

The case $R = 0$ gives back the RS solution, while the limiting case $R \rightarrow \infty$ produces the solution called Full Replica Symmetry Breaking (FRSB or ∞ -RSB) solution [44, 45]. In this limit $q_u - q_{u-1} \rightarrow 0$ for $u = 1, \dots, R$, and the matrix q_{ab} is described by a continuous, non-decreasing function $q(x)$, where, in the Parisi parameterization, x varies between 0 and 1. Solutions with a finite value of R are called R -RSB solutions [45, 5, 40, 41, 6]. These solutions can be described by a step-like function $q(x)$. Mixed-type solutions, with both discontinuous R -RSB-type and continuous FRSB-type parts for some x interval, are also possible [19, 20].

Inserting the form (21) into the free energy functional $G[q, m]$, eq. (13), with $m_a = m$, one obtains

$$\begin{aligned} \frac{2}{n} G[q, m] = & -g(1) - \sum_{u=0}^R (p_u - p_{u+1}) g(q_u) - \ln(1 - q_R) \\ & - \sum_{u=1}^R \frac{1}{p_u} \ln \frac{\hat{q}_u}{\hat{q}_{u+1}} - \frac{q_0 - m^2}{\hat{q}_1} - 2\kappa(m) \end{aligned} \quad (22)$$

where \hat{q}_u is the Replica Fourier Transform (RFT) of q_{ab} [46, 47]:

$$\hat{q}_u = \sum_{v=u}^{R+1} p_v (q_v - q_{v-1}). \quad (23)$$

The free energy functional can be conveniently expressed by introducing the auxiliary function

$$x(q) = p_0 + \sum_{u=0}^R (p_{u+1} - p_u) \theta(q - q_u) \quad (24)$$

which gives the fraction of pair of replicas with overlap $q_{ab} \leq q$. In terms of $x(q)$ the functional $G[q, m]$ takes the form

$$\frac{2}{n} G[q, m] = - \int_0^1 dq x(q) \Lambda(q) - \int_0^{q_R} \frac{dq}{\chi(q)} - \ln(1 - q_R) + \frac{m^2}{\chi(0)} - 2\kappa(m) \quad (25)$$

where

$$\chi(q) = \int_q^1 dq' x(q'). \quad (26)$$

Note that $\chi(q_u) = \hat{q}_{u+1}$ and, moreover, $\chi(q) = \chi(q_0) = \chi(0)$ for $0 \leq q \leq q_0$ since $x(q) = 0$ for $q \in [0, q_0]$.

The stationary point equations are obtained from the first variation of the free energy functional $G[q, m]$ with respect to $x(q)$ and m :

$$\frac{2}{n} \delta G[q, m] = - \int_0^1 dq F(q) \delta x(q) - 2 \left[b(m) - \frac{m}{\chi(0)} \right] \delta m \quad (27)$$

where

$$F(q) = \Lambda(q) - \int_0^q \frac{dq'}{\chi(q')^2} + \frac{m^2}{\chi(0)^2} \quad (28)$$

and

$$\delta x(q) = \sum_{u=1}^R [\theta(q - q_{u-1}) - \theta(q - q_u)] \delta p_u - \sum_{u=0}^R (p_{u+1} - p_u) \delta(q - q_u) \delta q_u. \quad (29)$$

Stationarity of $G[q, m]$ with respect to variations of m , q_u and p_u gives:

$$m = \chi(q_0) b(m) \quad (30)$$

$$F(q_u) = 0, \quad u = 0, \dots, R \quad (31)$$

$$\int_{q_{u-1}}^{q_u} dq F(q) = 0, \quad u = 1, \dots, R. \quad (32)$$

The function $F(q)$ is continuous, thus eqs. (31) and (32) require that between any two successive pairs (q_{u-1}, q_u) there must be at least two extrema of $F(q)$. Denoting these by q^* , the extrema condition $F'(q^*) = 0$ implies that

$$\int_{q^*}^1 dq x(q) = \frac{1}{\sqrt{\Lambda'(q^*)}} \quad (33)$$

where the prime denotes the derivative with respect to the argument q . The function $x(q)$ is a non-decreasing function of q , and the left hand side of this equation is, thus, a concave function. The solutions to this equation, thus, depend from the convexity properties of $1/\sqrt{\Lambda'(q)}$: in the region where it is concave a continuum of solution can be found, while where it is convex only discrete solutions exist. In the first case we deal with a continuous solution of the FRSB-type, while in the second case with a R-RSB-type solution. If $1/\sqrt{\Lambda'(q)}$ changes concavity for different intervals of q , we have a mixed-type solution.

In the above argument the presence of *the ordered part of the Hamiltonian does not play any role, once encoded into $b(m)$* . In this way one can decouple the computation studying the behavior of a model in a (self-induced) “external” field apart from the relationship between the field and the magnetizations induced by the ferromagnetic couplings.

The value of the field only enters in setting the value of q_0 , the lowest possible value of $q(x)$. As a consequence, the value b of $b(m)$ fine-tunes the range $[q_0, q_R]$ where solutions of the stationary point equations must be searched. Since q_0 is an increasing function of b the presence of an effective field b can only reduce the “complexity” of the solution found in absence of it. In particular, by increasing the value of b we can eventually force $q_0 = q_R$, that is a transition to the RS solution. For larger value of b only the RS solution exists.

If terms besides the $k = 1$ term (the uniform external field) are present in the ordered part of the Hamiltonian, cf. Eq. (9), what we just said is only part of the game. In this case, indeed, $b(m)$ is a function of m , and we must consider the possible solutions to Eq. (30) such that

$$b(m) = b \quad (34)$$

to unfold the complete solution. The unfolding depends on the form of $b(m)$. Therefore, starting from the same phase diagram expressed as function of b , different phase diagrams can be produced in the coupling constants, depending on the actual $b(m)$. An explicit instance of complete phase diagrams in T , $J^{(s,p)}$ and $J_0^{(s,p)}$ can be found in Ref. [26] and the cases $2+p$ ($p \geq 4$) and $3+4$ will be reported in Section 8. In the forthcoming part of the paper we shall, instead, address the fate of the different type of solutions as the value of the effective

field is varied. To illustrate the results, we shall study $s + p$ models in presence of an external uniform field b described by the stationary point equations (18), (19). Stability of the stationary point requires that the quadratic form

$$-\sum_{ab} \Lambda'(q_{ab}) (\delta q_{ab})^2 + \text{Tr} \left(\mathbf{q}^{-1} \delta \mathbf{q} \right)^2, \quad (35)$$

must be positive (semi)definite, where $\delta q_{ab} = \delta q_{ba}$ is the fluctuation of q_{ab} from the stationary point value.

3. The Spherical $s + p$ model in an uniform external field

The Spherical $s + p$ model is the particular model obtained from the general Hamiltonian (1) in which one retains only two terms with random s -spin and p -spin interactions and a ($k = 1$) uniform external field in Eq. (1). Without loosing in generality, we assume $s < p$ from now on. For this model we have:

$$\begin{aligned} g(q) &= \frac{\mu_s}{s} q^s + \frac{\mu_p}{p} q^p, \quad \Lambda(q) = \mu_s q^{s-1} + \mu_p q^{p-1}, \\ \kappa(m) &= bm \end{aligned} \quad (36)$$

The phase diagrams in the plane (μ_p, μ_s) , i.e. for $b = \beta h = 0$, are well known [20]. Depending on the value of s and p different type of solutions can be found, of both FRSB and R-RSB type and mixed. Since we are interested on the effect of the external field b on these different phases, it can be useful to use the following parametrization

$$\Lambda(q) = \mu_p (r q^{s-1} + q^{p-1}) \quad (37)$$

where

$$r = \frac{\mu_s}{\mu_p} = \frac{s}{p} \frac{J_s^2}{J_p^2}, \quad 0 \leq r < \infty \quad (38)$$

gives the relative strength of the s and p interaction terms, and we use μ_p and b as free parameter for given r . The temperature, when needed, is computed as $T/J_p = \sqrt{p/(2\mu_p)}$.

3.1. The RS Solution

All models, regardless of the value of s and p , for large enough temperature (i.e., small enough μ_s and μ_p) present a RS phase. The equation for the RS phase are obtained inserting

$$x(q) = \theta(q - q_0) \quad (39)$$

into equations (30), (31) and (32), or into the functional (25), then making it stationary with respect to m and q_0 . In either cases one ends up with:

$$m = (1 - q_0)^2 b \quad (40)$$

and

$$\Lambda(q_0) = \frac{q_0}{(1-q_0)^2} - b^2 \quad (41)$$

The RS phase remains stable as long as the relevant eigenvalue Λ_1 of the fluctuations remains positive:

$$\Lambda_1 = -\Lambda'(q_0) + \frac{1}{(1-q_0)^2} \geq 0. \quad (42)$$

Using the stationary point equation (41) one obtains the equivalent condition

$$\Lambda(q_0) - q_0 \Lambda'(q_0) + b^2 \geq 0. \quad (43)$$

The equal sign defines the critical line on which the RS phase ends. With the help of the parameterization (37) the parametric equation of the critical line reads:

$$\left\{ \begin{array}{l} \mu_p = \frac{1}{(1-q_0)^2} \frac{1}{r(s-1)q_0^{s-2} + (p-1)q_0^{p-2}} \\ \mu_s = r \mu_p \\ b^2 = \frac{1}{(1-q_0)^2} \frac{r(s-2)q_0^{s-1} + (p-2)q_0^{p-1}}{r(s-1)q_0^{s-2} + (p-1)q_0^{p-2}} \end{array} \right. \quad 0 \leq q_0 \leq 1 \quad (44)$$

Depending on the values of μ_p and μ_s , the curve may show points where

$$\left. \frac{d\mu_p}{db} \right|_{\mu_s/\mu_p} = 0, \quad (45)$$

that is $dT/dh = 0$ in the (h, T) plane. When present, one of such critical points occurs where the transition between the RS phase and the RSB one changes from continuous to discontinuous. A discontinuity of finite height appears in $q(x)$ at the transition and the critical line (44) stops there.

By using the parametric form (44), the points where $d\mu_p/db = 0$ correspond to the value of q_0 solution of

$$2\Lambda'(q_0) + (q_0 - 1)\Lambda''(q_0) = 0. \quad (46)$$

The largest solution $0 \leq q_c < 1$ of this equation, when it exists, gives the critical point where the line (44) ends, and q_0 gets restricted to $q_c \leq q_0 \leq 1$. For $r = 0$ we recover $q_c = 1 - 2/p$, while it is $q_c = 1 - 2/s$ in the opposite limit $r \rightarrow \infty$. This is the critical value of the *pure* p -spin, or s -spin, spherical model. Beyond this point one must resort to a 1RSB Ansatz in order to obtain the expression for the transition line.

3.2. The 1RSB Solution

The 1RSB phase is described by a function $x(q)$ of the form

$$x(q) = x\theta(q - q_0) + (1 - x)\theta(q - q_1) \quad (47)$$

with $x \in [0, 1]$ and $0 \leq q_0 < q_1 \leq 1$. By plugging this expression into the free energy functional $G[q, m]$ (25), and equating to zero its derivatives with respect to q_0 , q_1 , x and m , or directly into the stationary point equations (30), (31) and (32), we obtain the 1RSB (static) equations

$$\Lambda(q_0) = \frac{q_0}{\chi(q_0)^2} - b^2 \quad (48)$$

$$\Lambda(q_1) - \Lambda(q_0) = \frac{q_1 - q_0}{\chi(q_1)\chi(q_0)} \quad (49)$$

$$g(q_1) - g(q_0) - \left[\frac{q_0 - m^2}{\chi(q_0)^2} - \frac{1}{x} \frac{1}{\chi(q_0)} \right] + \frac{1}{x^2} \ln \left[\frac{\chi(q_1)}{\chi(q_0)} \right] = 0 \quad (50)$$

and

$$m = \chi(q_0)b \quad (51)$$

where

$$\chi(q_1) = 1 - q_1, \quad \chi(q_0) = 1 - q_1 + x(q_1 - q_0). \quad (52)$$

For the purpose of the (numerical) solution of these equations, it is convenient to transform eq. (50) into the equivalent expression

$$2 \frac{g(q_1) - g(q_0) - \Lambda(q_0)(q_1 - q_0)}{(q_1 - q_0)[\Lambda(q_1) - \Lambda(q_0)]} = z(y) \quad (53)$$

where $y = \chi(q_0)/\chi(q_1) \in [0, 1]$ and

$$z(y) = -2y \frac{1 - y - \ln y}{(1 - y)^2} \quad (54)$$

is the CS z -function [5]. The advantage of equation (53) over (50) is that it does not depend on temperature. With the parameterization (37) it depends only on the ratio $r = \mu_s/\mu_p$. We can then easily solve the 1RSB equations for fixed r , and x . The procedure is quite standard. One first introduces the ratio $t = q_0/q_1 \in [0, 1]$ to be used as free parameter, and rewrite

$$q_1 = \frac{1 - y}{1 - y + xy(1 - t)}, \quad \chi(q_0) = \frac{x(1 - t)}{1 - y + xy(1 - t)}. \quad (55)$$

and $q_0 = tq_1$, $\chi(q_1) = y\chi(q_0)$. With this replacements eq. (53) becomes function of y and t , besides r and x . Next one fixes the values of r and x , and solve equation (53) for y by varying $t \in [0, 1]$. In this way one obtains $y \equiv y(t; x, r)$, that plugged into eqs. (49) and (48) gives the corresponding $\mu_p(t; x, r)$ and

$b(t; x, r)$. This procedure builds the x -line for the 1RSB phase in the space (μ_p, μ_s, b) on the plane $r = \mu_s/\mu_p$.

The x -line with $x = 1$ plays a special role. This line is the critical line separating the 1RSB and RS phases. The transition is discontinuous in $q(x)$ along the whole line since $t = q_0/q_1 < 1$, and becomes continuous only at the end point $t \rightarrow 1$.

The stability analysis of the 1RSB stationary point shows that the 1RSB solution is stable provided the eigenvalues

$$\Lambda_1^{(1)} = -\Lambda'(q_1) + \frac{1}{\chi(q_1)^2} \quad (56)$$

$$\Lambda_0^{(3)} = -\Lambda'(q_0) + \frac{1}{\chi(q_0)^2} \quad (57)$$

are both positive.

To illustrate the phases and the transition we shall now consider some explicit examples.

4. The 3 + 4 model

This model is the prototype of a system with only RS and 1RSB phases separated by a discontinuous transition line. Indeed for $s = 3$, $p = 4$ and $b = 0$ eq. (43) reduces to

$$-\mu_3 q_0^2 - 2\mu_4 q_0^3 \geq 0 \quad (58)$$

that can be satisfied only for $q_0 = 0$. For $q_0 = 0$ the eigenvalue Λ_1 , eq. (42), reduces to $\Lambda_1 = 1 > 0$, and RS solution with $q_0 = 0$ is stable everywhere for $b = 0$ [20]. However, for large enough μ_3 and μ_4 a 1RSB phase with a favorable free energy appears. The transition between the two phases occurs along the x -line with $x = 1$. The bottom-left inset in Figure 1 shows the phase diagram of the model for $b = 0$.

The phase diagram in the full (μ_4, μ_3, b) space is reported in Figure 1. The lines, drawn for different values of r , define the critical surface separating the RS phase from the 1RSB phase. The transition between the two phases is continuous on the part of the critical surface spanned by the full lines. This means that the difference $q_1 - q_0$ vanishes when approaching this portion of critical surface from the 1RSB side. The breaking parameter x takes a value between 0 and 1 depending on the intersection point. The transition turns into a discontinuous transition on the dashed part of the critical surface. Here the difference $q_1 - q_0$ remains finite as the critical surface is approached from the 1RSB side, but $x = 1$. Indeed, the discontinuous part of the critical surface is the surface spanned by the x -lines with $x = 1$ for different r . The two parts of the critical surface join each other along the end point line, where $d\mu_4/db|_r = 0$. Along this line

$$q_0 = q_1 = q_c = \frac{1}{12} \left[3(1 - r) + \sqrt{9r^2 + 6r + 9} \right], \quad r \in [0, \infty). \quad (59)$$

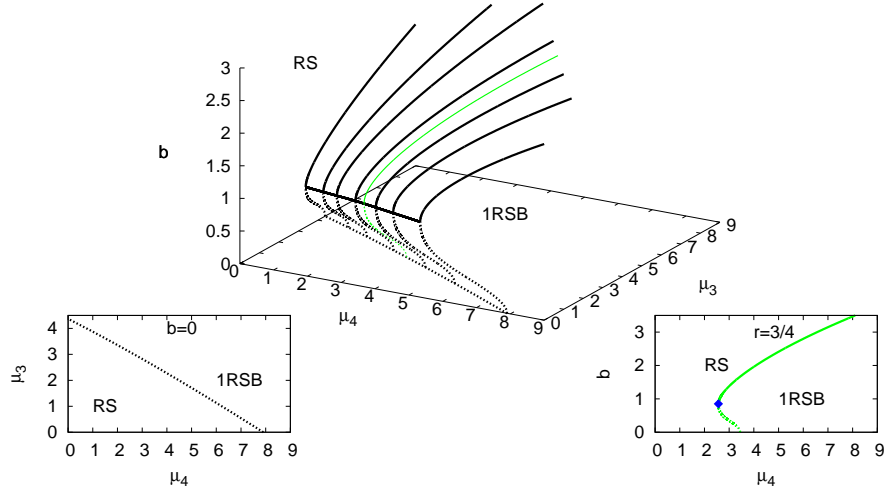


Figure 1: Phase diagram of the 3 + 4 model in the (μ_4, μ_3, b) space (center). The lines are the critical lines drawn for different values of r . Full black line: continuous transition; Dashed black line: discontinuous transition. The discontinuous and continuous transition surfaces join on the end point line where $d\mu_3/db|_r = 0$. Left inset: projection on the $b = 0$ plane. Right inset: projection on the $r = 3/4$ plane (grey lines, green online); the dot is the end point $d\mu_4/db|_r = 0$.

and

$$\mu_4 = \frac{1}{(1 - q_c)^2} \frac{1}{2rq_c + 3q_c^2} \quad (60)$$

$$b^2 = \frac{1}{(1 - q_c)^2} \frac{rq_c + 2q_c^2}{2rq_c + 3q_c^2} \quad (61)$$

while $\mu_3 = r\mu_4$

In the bottom-right inset of Figure 1 we report a slice of the phase diagram taken for fixed $r = 3/4$, though the plot is generic for all r . It is similar to the phase diagram of the *pure* p -spin spherical model in an external field. Indeed, by varying r we smoothly interpolate between the *pure* 3-spin and 4-spin spherical model in a field.

The scenario just described remains valid for all values of $p > s > 3$, provided the difference $p - s$ is not too large.¹

5. The 2 + 3 model

In the 3 + 4 model the transition between the RS and 1RSB phases at small fields is always discontinuous. Next in phase diagram complexity sits the 2 + 3 model. For $b = 0$ this model possesses a phase diagram with only RS and 1RSB

¹When $s \ll p$ a 2RSB phase arises in the frozen phase [6, 7].

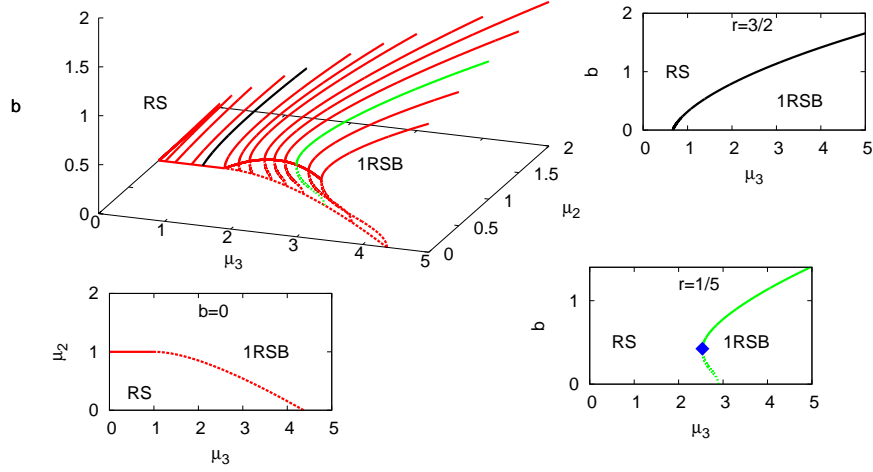


Figure 2: Phase diagram of the 2 + 3 model in the (μ_3, μ_2, b) space. The lines are the critical lines drawn for different values of r . Full line (red online): continuous transition; dotted line (red online): discontinuous transition; the end point line joining the discontinuous and continuous critical surfaces hits the $b = 0$ plane at the point $(1, 1, 0)$. Bottom (left) inset: $b = 0$ projection; the transition between the RS and the RSB phases is continuous along the full line, and discontinuous along the dotted line. Two x -lines of the 1RSB are also shown. All x -lines ends on the continuous transition line where $q_1 = q_0 = 0$ and $\Lambda_1 = \Lambda_0^{(3)} = 0$. Top (right) inset: projections on $r = 3/2$ (light grey full and dotted lines, green online) and $r = 1/5$ (black line) planes, from bottom to top. For $r < 1$ the discontinuous line merge into a continuous line (red dot). At $r = 1$ the continuous transition line hits the μ_3 axis with an infinite slope. For $r > 1$ no discontinuous transition exists.

phases but, at difference with the 3 + 4 model, the transition can be either continuous or discontinuous, see the bottom-left inset of Figure 2.

When $s = 2$, and p generic, the stability condition (43) for $b = 0$ becomes

$$-\mu_p(p-2)q_0^{p-1} \geq 0 \quad (62)$$

that again is satisfied only for $q_0 = 0$. However, at difference with the 3 + 4 case, the relevant eigenvalue now reads $\Lambda_1 = 1 - \mu_2$, and vanishes for $\mu_2 = 1$. Along this line the RS phase ($\mu_2 < 1$) becomes unstable against a 1RSB phase ($\mu_2 > 1$), and a continuous transition between the two phases occurs. The continuous transition line ends at the point $(\mu_3, \mu_2) = (1, 1)$ where the line hits the 1RSB x -line with $x = 1$ [19, 20].

Figure 2 shows the phase diagram of the 2 + 3 model in the space (μ_3, μ_2, b) . The RS and 1RSB phases are separated by a critical surface. The transition can be either continuous, on surface spanned by full lines, or discontinuous, on surface spanned by dotted lines. The continuous and discontinuous parts of the critical surface are joint along the end point line where $d\mu_3/db|_r = 0$. Here

$$q_0 = q_1 = q_c = \frac{1-r}{3}, \quad r \leq 1 \quad (63)$$

and

$$\mu_3 = \frac{1}{(1-q_c)^2} \frac{1}{r+2q_c} \quad (64)$$

$$b^2 = \frac{1}{(1-q_c)^2} \frac{q_c^2}{r+2q_c} \quad (65)$$

while $\mu_2 = r \mu_3$.

For $r > 1$ the transition between the RS and 1RSB phases can only take place continuously, with $q_0 - q_1 \rightarrow 0$ on the critical surface. In Figure 2, we show slices of the phase diagram on the planes of constant r above and below the critical value of $r = 1$.

6. Full RSB

Moving to models more complicated than those mentioned above one can study the RSB in its continuous limit, as introduced by Parisi to solve the Sherrington-Kirkpatrick model. That is, even in spherical models, one finds glassy phases whose correct thermodynamics can be computed only in this limit. The FRSB phase is described by a continuous order parameter function $q(x)$ of the form

$$q(x) = \begin{cases} q_0 = q(x_0) & 0 \leq x \leq x_0 \\ q(x) & x_0 \leq x \leq x_1 \\ q_1 = q(x_1) & x_1 \leq x < 1 \end{cases} \quad (66)$$

see Figure 3, solution of the stationary point equations

$$\Lambda(q_0) = \frac{q_0}{\chi(q_0)^2} - b^2 \quad (67)$$

$$\Lambda(q) - \Lambda(q_0) = \int_{q_0}^q \frac{dq'}{\chi(q')^2}, \quad q_0 \leq q \leq q_1 \quad (68)$$

with $\chi(q)$ given by eq. (26). To solve these equations we take the derivative of eq. (68) with respect to q , leading to

$$\Lambda'(q) = \frac{1}{\chi(q)^2}, \quad q_0 \leq q \leq q_1. \quad (69)$$

By using this relation into eq. (67) we obtain the equation

$$b^2 = \frac{q_0}{\chi(q_0)^2} - \Lambda(q_0) = q_0 \Lambda'(q_0) - \Lambda(q_0) \quad (70)$$

that solved for $q_0 = q_0(b)$ (or $b = b(q_0)$) fixes the lower bound of $q(x)$. To find the continuos part of $q(x)$ we observe that from the definition of $\chi(q)$, eq. (26), simply follows that $\chi'(q) = -x(q)$. As a consequence taking the derivative of the relation (69) we have

$$\Lambda''(q) = -\frac{2}{\chi(q)^3} \chi'(q) \Rightarrow x(q) = \frac{1}{2} \frac{\Lambda''(q)}{[\Lambda'(q)]^{3/2}}, \quad q_0 \leq q \leq q_1 \quad (71)$$

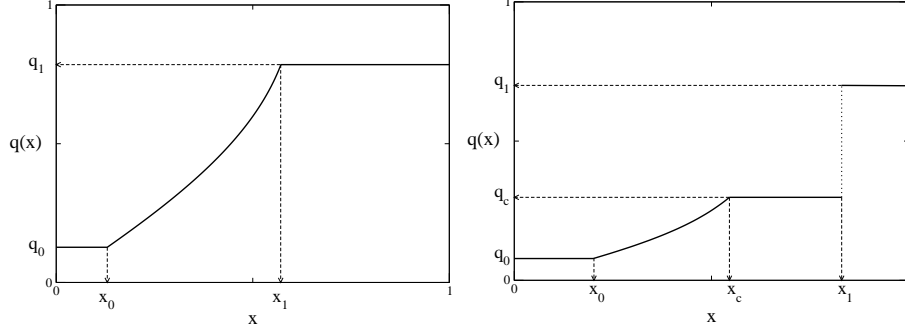


Figure 3: Schematic form of the order parameter function $q(x)$ in the FRSB (left) and 1FRSB (right) phases. As $q_c = q_1$ the two functions have equal form.

which gives the explicit analytic form of $x(q)$. Once inverted, it leads to the continuous part of $q(x)$. Inserting now the value of $q_0 = q_0(b)$ obtained from eq. (70) into $x(q)$ from eq. (71) we have $x_0 = x(q_0) = x_0(b)$.

To find the upper bound value q_1 of $q(x)$, and x_1 , we observe that $\chi(q_1) = 1 - q_1$. As a consequence, from eq. (69) evaluated for $q = q_1$ we obtain

$$\Lambda'(q_1) = \frac{1}{(1 - q_1)^2} \quad (72)$$

that fixes the value of q_1 . The value of x_1 follows as $x_1 = x(q_1)$.

6.1. The 1FRSB Solution

The 1FRSB solution differs from the FRSB for the presence of a discontinuous part in the order parameter function $q(x)$:

$$q(x) = \begin{cases} q_0 = q(x_0) & 0 \leq x \leq x_0 \\ q(x) & x_0 \leq x \leq x_c \\ q_c = q(x_c) & x_c \leq x < x_1 \\ q_1 & x_1 \leq x < 1 \end{cases} \quad (73)$$

as schematically shown in the right side of Figure 3. The stationary point equations for the 1FRSB are a “mix” of those for the 1RSB and FRSB, and read:

$$\Lambda(q_0) = \frac{q_0}{\chi(q_0)^2} - b^2 \quad (74)$$

$$\Lambda(q) - \Lambda(q_0) = \int_{q_0}^q \frac{dq'}{\chi(q')^2}, \quad q_0 \leq q \leq q_c \quad (75)$$

$$\Lambda(q_1) - \Lambda(q_c) = \frac{q_1 - q_c}{\chi(q_1)\chi(q_c)} \quad (76)$$

where, see eq. (26),

$$\chi(q_1) = 1 - q_1, \quad \chi(q_c) = 1 - q_1 + x_1(q_1 - q_c) \quad (77)$$

and

$$\chi(q) = 1 - q_1 + x_1(q_1 - q_c) + \int_q^{q_c} dq' x(q'), \quad q_0 \leq q \leq q_c. \quad (78)$$

The position of the breaking point x_1 follows from the equation

$$2 \frac{g(q_1) - g(q_c) - (q_1 - q_c)\Lambda(q_c)}{(q_1 - q_c)[\Lambda(q_1) - \Lambda(q_c)]} = z(y) \quad (79)$$

where $y = \chi(q_c)/\chi(q_1) \in [0, 1]$.

The 1FRSB solution reduces to the FRSB solution for $q_c = q_1$ or $x_1 = 1$. In the former case the transition is continuous, and discontinuous in the latter. When $q_0 = q_c$ the 1FRSB solution goes over a 1RSB solution.

Similar to the FRSB solution, only q_0 (and $x_0 = x(q_0)$) depends on b . All other quantities remain unchanged by varying b . As a consequence, since q_0 grows with b (with μ_p 's held fixed) eventually $q_0 = q_c$ and we observe a transition between the 1FRSB and the 1RSB phases.

7. The $2 + p$ model

The prototype model with both FRSB and 1FRSB phases is the $2 + 4$ spherical model. The model belongs to the family of $2 + p$ spherical models with $p > 3$ whose phase diagram presents RS, 1RSB, FRSB and 1FRSB phases. The phase diagram reproduced in the full (μ_4, μ_2, b) space is shown in Figure 4, where the four different phases and relative transition lines are indicated. Its $b = 0$ projection is shown in the bottom-left inset.

We now discuss the conduct of each phase when the field b is switched on. We first analyze the FRSB and 1FRSB phases, then the RS phase, and, eventually, the 1RSB phase.

Critical r_x^t values	Phases (transition kinds)
$r_0^{(1)} = 6$	RS, FRSB (continuous) — — — —
$r_0^{(0)} = 0.6382$	RS, FRSB, 1FRSB (continuous) — — — —
$r_1^{(1)} = 0.375$	RS, 1RSB, FRSB, 1FRSB (continuous) — — — —
$r_1^{(0)} = 0.2378$	RS, 1RSB, FRSB, 1FRSB (cont. and disc.) — — — —
	RS, 1RSB (cont. and disc.)

Table 1: Boundary values of $r = \mu_2/\mu_4$ between different kinds of (μ_4, b) phase diagrams. The top index in $r_x^{(t)}$ is the value of $t = q_0/q_1 = 0, 1$, the sub-index is the value of $x = 0, 1$. See Fig. 4 for a graphical representation.

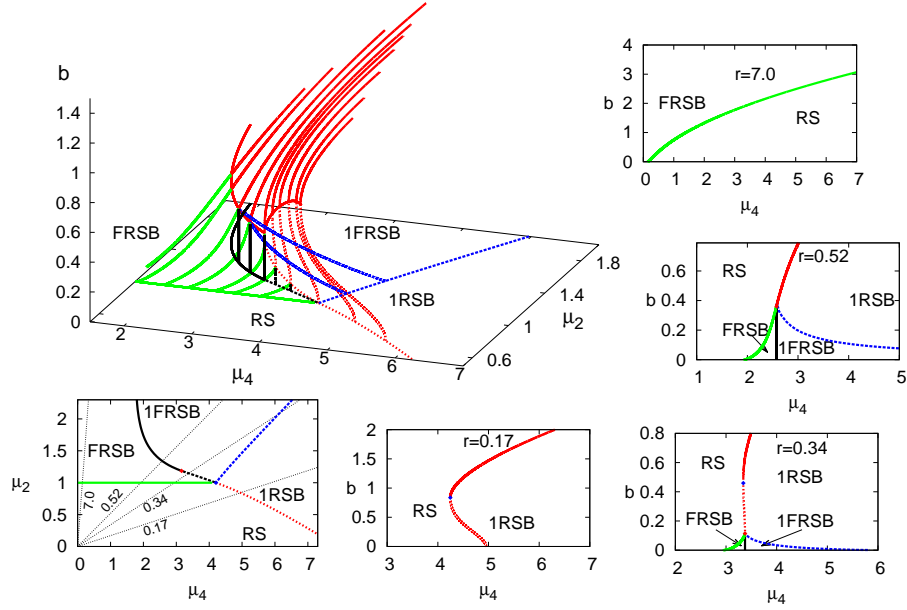


Figure 4: Phase diagram of the 2 + 4 model in the μ_2, μ_4, b space. Dark grey full line (red online): RS-1RSB continuous transition. Dark grey dotted line (red online): RS-1RSB discontinuous transition. Grey dashed line (blue online): 1RSB-1FRSB continuous transition. Light grey full line (green online): RS-FRSB continuous transition. Black full line: FRSB-1FRSB continuous transition. Black dashed line: FRSB-1FRSB discontinuous transition. Bottom Left: $b = 0$ projection. On the FRSB-1FRSB transition line (black) $q_c = q_1$, while on the 1FRSB-1RSB transition line (dashed grey/blue) $q_c = 0$. The transition line between the RS and the 1RSB phases (dark grey/red dotted) is the x -line with $x = 1$. The tiny dotted black lines on the $b = 0$ plane denote different values of the (μ_4, b) plane at fixed $r = \mu_2/\mu_4$. Each plot is generic for a given interval of r values. Boundary values are shown in Tab. 1. From Top Right to Bottom Mid, clockwise: phase diagrams of the 2 + 4 model in the plane (μ_4, b) with fixed $r = 7.0, 0.52, 0.34$ and 0.17 .

7.1. 2 + p: FRSB phase

The FRSB solution is known to reproduce the low temperature phase of the 2 + p model at $b = 0$ [48]. In this special case, equations (67)-(71) become:

$$q_0 = \left[\frac{b^2}{\mu_p(p-2)} \right]^{1/(p-1)} \quad (80)$$

$$x(q) = \frac{1}{2} \frac{\mu_p(p-1)(p-2)q^{p-3}}{[\mu_2 + \mu_p(p-1)q^{p-2}]^{3/2}} \quad (81)$$

$$\mu_2 + \mu_p(p-1)q_1^{p-2} = \frac{1}{(1-q_1)^2} \quad (82)$$

At $b > 0$ the FRSB may exist only if the ratio $r = \mu_2/\mu_p$ is larger than the critical value $r_1^{(0)}$, cf. Tab. 1. When the field b is switched on only q_0 is modified: it becomes non-zero and grows with $b^{2/(p-1)}$, c.f.r equation (80). Increasing b

for fixed μ_2 and μ_p , we eventually have $q_0 = q_1$ and a continuous transition from the FRSB to the RS phase takes place. In Figure 4 the RS-FRSB critical surface for the $p = 4$ case is the one spanned by the light grey (green) lines. For any (μ_4, b) slice with $r > r_0^{(1)}$ the FRSB phase is bounded exclusively by the RS phase, see top inset of Fig. 4. At $r = r_0^{(1)}$ a boundary with the 1FRSB phase first appears, the relative critical surface is the one spanned by the black lines in Fig. 4. The transition can be either continuous, if $r_1^{(1)} < r < r_0^{(1)}$ (full continuous lines, see also the inset for $r = 0.52$ in Fig. 4), or discontinuous, if $r_1^{(0)} < r < r_1^{(1)}$ (dashed lines, cf. inset of Fig. 4 for $r = 0.34$).

7.2. $2 + p$: 1FRSB phase

The 1FRSB phase may exist only if $r_1^{(0)} < r < r_0^{(1)}$, cf. Tab. 1. The fate of the 1FRSB phase in a field is similar to that of the FRSB phase because the field b only affects the value of $q_0 \sim b^{2/(p-1)}$. As a consequence, for b large enough, $q_0 = q_c$ and the 1FRSB phase goes over the 1RSB phase. The transition is clearly continuous. The 1FRSB-1RSB surface is the one spanned by the grey (blue) dashed lines in Fig. 4 and insets. The other boundary of the 1FRSB phase is with the FRSB phase. The transition between these two phases can be either discontinuous or continuous, depending on r being smaller or larger than $r_1^{(1)}$, as we mentioned above, discussing the FRSB phase. We note that for $b = 0$ the 1FRSB phase is bounded by the 1RSB phase only when $r_1^{(0)} < r < r_0^{(0)}$. See, in Fig. 4 the insets for $r = 0.52$ and $r = 0.34$.

7.3. $2 + p$: RS phase

The field b has an ordering effect on the system, i.e., for large value of b the RS phase is the stable phase, c.f. eq. (43). When b is decreased the disordered terms in the Hamiltonian become more and more relevant and, depending on the value of μ_2 and μ_p , the RS phase may become unstable towards a more complex phase. This happens when the relevant eigenvalue Λ_1 becomes negative, see eq. (42). The vanishing of Λ_1 defines the critical RS surface, whose parametric equation is given by eq. (44) for $s = 2$. In Figure 4 for $p = 4$ this surface is the one spanned by the light grey (green online) and dark grey (red) full lines. If the value of b is further decreased one enters into either the FRSB phase, crossing the light grey (green) lines in figure, or the 1RSB phase, crossing the full dark grey (red) lines in figure. The transition is in either case continuous. Which phase may be reached as the field b varies depends on the ratio r between the coupling coefficients μ_2 and μ_p . For $r > r_0^{(1)}$ only the FRSB phase can be encountered, see top inset of Fig. 4 for $p = 4$, while for $r < r_1^{(0)}$ only the 1RSB phase is feasible: see bottom inset of Fig. 4. In between ($r_0^{(1)} > r > r_1^{(0)}$) both 1RSB and FRSB are possible, see insets for $r = 0.34$ and $r = 0.52$ in Fig. 4.

The continuous RS critical surface may bend, and become multivalued, if $d\mu_p/db = 0$ for fixed r . This occurs when q_0 equals the largest solution $0 < q_c(r) < 1$ of

$$f(q) = p(p-1)q^{p-2} - (p-1)(p-2)q^{p-3} + 2r = 0, \quad (83)$$

c.f. eq. (46) for $s = 2$. For large enough r this equation has no physical solutions. They do appear when r is sufficiently small. For $r = 0$ we have $q_c(0) = (p-2)/p$. To find the critical value of r we observe that $f(q) \sim -(p-1)(p-2)q^{p-3}$ for $q \simeq 0^+$ while $f(q) \sim p(p-1)q^{p-2}$ for $q \gg 1$. Hence, there must be at least one minimum $f'(q^*) = 0$ with $q^* > 0$. A simple calculation yields $q^* = (p-3)/p$. This, with $f(0) = 2r$, implies that, if r is not too large, equation (83) has at least two solutions with $q > 0$, and the surface may bend. Since increasing r shifts $f(q)$ upwards, a crossover value of r is obtained by imposing that $f(q^*) = 0$. This leads to

$$r_1^{(1)} = \frac{(p-1)(p-3)^{p-3}}{2p^{p-3}} \quad (84)$$

The value $q_c(r)$ for $r < r_1^{(1)}$ defines the end point line where the surface bends. For the special case $2 + 4$ reported in Fig. 4, eq. (83) can be explicitly solved and one finds

$$q_c(r) = \frac{1}{12} [3 + \sqrt{9 - 24r}], \quad r < r_1^{(1)} = 3/8. \quad (85)$$

When the continuous RS critical surface bends, the transition between the RS and the 1RSB phases becomes discontinuous on the end point line $q_c(r)$. This line is the dark grey (red) line joining the contact points between the full and dotted dark grey (red) lines in Figure 4. Below this line the transition between the RS and 1RSB is discontinuous and occurs on the critical surfaces spanned by the x -line of the 1RSB phase with $x = 1$. This is represented by dark grey dotted lines in figure 4 (see insets for $r = 0.17, 0.34$).

We note that since the surface is bended there is an inverse transition in b . That is, by decreasing b we can enter the 1RSB phase from the RS phase via a continuous transition and, decreasing further b , leave the 1RSB phase for the RS phase again via a discontinuous transition.

7.4. $2 + p$: 1RSB phase

The 1RSB phase is found for large enough μ_2 and μ_p , see e.g. the bottom-left inset of Fig. 4 for the $2 + 4$ model with $b = 0$. When b increases q_0 grows and eventually becomes equal to q_1 . Here the 1RSB phase ends. Since as $q_0 \rightarrow q_1$ the second 1RSB equation (49) reduces to the critical condition $\Lambda_1 = 0$ of the RS phase, c.f. eq. (42), one enters into the RS phase through the continuous RS-1RSB transition, the surface spanned by the dark grey (red) full lines in Fig. 4. This critical surface bounds the 1RSB from "above".

As discussed for the RS phase, if the ratio r between μ_2 and μ_p is smaller than the critical value $r_1^{(1)}$ the critical surface $\Lambda_1 = 0$ bends. Where this happens the transition between the 1RSB and RS phases takes place with a finite value of $q_1 - q_0$ and occurs when we cross the surface spanned by the $x = 1$ lines of the 1RSB solution. In Fig. 4 this is represented by the surface spanned by the dark grey (red) dotted lines.

If the ratio r exceeds the critical value $r_1^{(0)}$ the eigenvalue $\Lambda_0^{(3)}$ may become negative for low b , and the 1RSB phase is unstable with respect to a 1FRSB

phase. The transition between the 1RSB and the 1FRSB phase occurs on the critical surface defined by $\Lambda_0^{(3)} = 0$.

This critical surface intersects the $b = 0$ plane along the critical line of equation, see Appendix A,

$$\mu_p = \frac{(1 - y_0 + xy_0)^p}{x^2 y (1 - y_0)^{p-3}} \quad (86)$$

$$\mu_2 = \frac{(1 - y_0 + xy_0)^2}{x^2}, \quad (87)$$

where y_0 solution of

$$z(y_0) = \frac{2 + (p - 2)y_0}{p}, \quad (88)$$

This is shown as dashed grey (blue) lines in Figure 4. Along this line the ratio $r = \mu_2/\mu_p$ is given by

$$r = \frac{y_0(1 - y_0)^{p-3}}{(1 - y_0 + xy_0)^{p-2}} \quad (89)$$

and varies between

$$r_1^{(0)} = y_0(1 - y_0)^{p-3} \quad (90)$$

for $x = 1$ and

$$r_0^{(0)} = \frac{y_0}{1 - y_0} \quad (91)$$

for $x = 0$. For r in this range both FRSB and 1FRSB phases, beside the 1RSB phase, may exist, see inset of Fig. 4 for $r = 0.34$.

When $x = 1$ the critical line intersects both the RS-1RSB and RS-FRSB critical lines at the multi-critical point. For $r < r_1^{(0)}$ only the RS and 1RSB phases exist, see inset of Figs 4 for $r = 0.17$.

In the opposite limit $x = 0$ both μ_p and μ_2 diverge, while its ratio r remains finite. As a consequence for $r > r_0^{(0)}$ only a 1RSB phase with $q_0 \neq 0$ may exist, provided $r < r_0^{(1)}$ (see below), cf. $r = 0.52$ inset of Fig. 4. The numerical values for $p = 4$ are: $y_0 = 0.389571$, $r_1^{(0)} = 0.2378$, $r_0^{(0)} = 0.63819$.

The breaking point x cannot exceed 1, implying that the 1RSB critical surface is bounded by the x -line with $x = 1$ (dark grey/red dotted line in Figure 4). This line intersects the $b = 0$ plane at the end point of the 1RSB-1FRSB critical line on the $b = 0$ plane and gives the continuation to $b \neq 0$ of the critical RS-1RSB line found on the $b = 0$ plane.

The other boundary of the 1RSB-1FRSB critical surface occurs when $q_1 = q_0$, and the discontinuity associated with the 1RSB (and 1FRSB) solution disappears. The equation of the critical end line of the 1RSB-1FRSB critical surface reads, see Appendix A,

$$\mu_p = \frac{2}{27} \frac{(p - 3 + 3x)^p}{(p - 1)(p - 2)(p - 3)^{p-3}x^2} \quad (92)$$

$$\mu_2 = \frac{p}{27} \frac{(p-3+3x)^2}{(p-2)x^2} \quad (93)$$

$$b^2 = \frac{2}{27} \frac{(p-3)^2(p-3+3x)}{(p-1)x^2}. \quad (94)$$

By varying x between 0 and 1 we obtain the critical line where the RS-1RSB-1FRSB-FRSB phases meet altogether. This is represented as a dark grey/red full line for $r > r_1^{(1)}$ in Figure 4, see also the $r = 0.52$ inset. Along this line the ratio r is given by

$$r = \frac{p(p-1)}{2} \frac{(p-3)^{p-3}}{(p-3+3x)^{p-2}} \quad (95)$$

varying between $r_1^{(1)}$, cf. Eq. (84) for $x = 1$, and

$$r_0^{(1)} = \frac{p(p-1)(p-3)^{p-4}}{2} \quad (96)$$

for $x = 0$.

When $x = 1$ the line meets the critical x -line with $x = 1$. Hence, a discontinuous RS-1RSB transition can be found only if $r < r_1^{(1)}$, while the transition is always continuous for $r > r_1^{(1)}$, as shown in the (μ_4, b) diagrams at fixed r in Fig. 4.

As it occurs along the 1RSB-1FRSB surface, for $x = 0$ both μ_p and μ_2 , as well as b , diverge. The ratio r , nevertheless, remains finite. As a consequence, the 1RSB phase cannot be found if $r > r_0^{(1)}$, and only the FRSB phase survive, see Fig. 4. For $p = 4$, $r_1^{(1)} = 3/8$ and $r_0^{(1)} = 6$.

8. Phase diagrams of the $s+p$ model in the ferromagnetic interaction strength

The spherical $s+p$ model with ferromagnetic interactions is the particular model described by

$$\Lambda(q) = \mu_s q^{s-1} + \mu_p q^{p-1}, \quad k(m) = b_s m^s + b_p m^p \quad (97)$$

where, as usual, it is assumed $p > s$.

Next to equations (37-38) it is convenient to introduce the parameterization

$$\kappa(m) = b_p (\gamma m^s + m^p) \quad (98)$$

where

$$\gamma = \frac{b_s}{b_p} = \frac{p! J_0^{(s)}}{s! J_0^{(p)}}, \quad 0 \leq \gamma < \infty \quad (99)$$

gives the relative strength of the s and p interaction terms, and use μ_p and b_p as free parameter for given r and γ . We do not consider the case of competing ferro-antiferromagnetic interaction ($\gamma < 0$), but the extension is straightforward.

With this parameterization the “unfolding equations” $b(m) = b$ and $m = \chi(q_0)b$, cf. equation (34) and Sec. 2.2, yield

$$\begin{aligned} b(m) &= \frac{m}{\chi(q_0)} \Rightarrow \\ b_p &= \frac{1}{\chi(q_0)} \frac{1}{\kappa'(m)/m} = \frac{1}{\chi(q_0)} \frac{1}{\gamma s m^{s-2} + p m^{p-2}} \end{aligned} \quad (100)$$

which, with eqs. (48)-(51), gives b_p as function of SG parameters $\mathbf{q} = \{q_0, q_1, \dots\}$ and $\underline{\mu} = \{\mu_p, \mu_s\}$ in the case of an uniform external field.

The *natural* parameters μ_p and b_p can be transformed into the *physical* parameters that give the temperature and the strength of the ferromagnetic part by setting

$$J_p^2 = \alpha J^2, \quad J_s^2 = (1 - \alpha) J^2, \quad \alpha = \frac{s}{s + rp} \quad (101)$$

and

$$J_0^{(p)} = \alpha_0 J_0, \quad J_0^{(s)} = (1 - \alpha_0) J_0, \quad \alpha_0 = \frac{p!}{p! + rs!} \quad (102)$$

where J and J_0 measure the overall strength of the disorder and ferromagnetic parts. One then has

$$\mu_p = \frac{p}{2} \alpha \beta^2 J^2 \Rightarrow T/J = \sqrt{\frac{p\alpha}{2\mu_p}} = \sqrt{\frac{sp}{2(s+rp)\mu_p}} \quad (103)$$

$$b_p = \frac{\alpha_0}{p!} \beta J_0 \Rightarrow J_0 = \frac{p!}{\alpha_0} T b_p = (p! + \gamma s!) T b_p. \quad (104)$$

For fixed temperature T , or μ_p , the Ferromagnetic (FM) solution $m \neq 0$ first appears at the critical value

$$J_0^* = \min_{q_0} J_0(\mathbf{q}, \underline{\mu}). \quad (105)$$

For $J_0 < J_0^*$ only the Paramagnetic (PM) solution $m = 0$ is possible.

The PM/FM transition can be either continuous or discontinuous in m . If the minimum of J_0 occurs for $q_0 = 0$,

$$J_0^* = J_0(q, \mu)|_{q_0=0} \equiv J_0^c \quad (106)$$

which corresponds to the case of zero external field in the associated model and hence $m = 0$, then

$$m \rightarrow 0 \text{ as } J_0 \rightarrow J_0^{c+} \quad (107)$$

and the PM/FM transition is *continuous*.

If, on the contrary, the minimum occurs at a finite value of q_0 , then $m \neq 0$ at J_0^* and the FM phase appears *discontinuously*. In this case the critical point J_0^* in general corresponds to a *spinodal* point, where the solution first appears. The true thermodynamic (discontinuous) transition occurs at $J_0^d \geq J_0^*$, where the free energy Φ of the PM and FM solutions become equal.

8.1. The $2 + p$ Model

From the form of the unfolding equation (100) we see that a continuous transition, i.e. a finite J_0^c , is possible only if $s = 2$, when the first m disappears from the denominator so that b_p is finite for $m = 0$:

$$b_p \Big|_{m=0} = \frac{1}{2\gamma\chi(0)} \quad (108)$$

leading to

$$J_0^c = \frac{2\gamma + p!}{2\gamma} \frac{T}{\chi(0)} \quad (109)$$

The explicit form of J_c depends on the structure of the solution of the associated problem with zero external field b . If for the given temperature T (or μ_p) the $b = 0$ phase is Replica Symmetric (RS) then $\chi(q_0) = 1 - q_0$, and

$$J_0^c = \frac{2\gamma + p!}{2\gamma} T, \quad (\text{RS}) \quad (110)$$

In the case of a one-step replica symmetry (1RSB) phase $\chi(q_0) = 1 - q_1 + x(q_1 - q_0)$ and

$$J_0^c = \frac{2\gamma + p!}{2\gamma} \frac{T}{1 - q_1 + xq_1}, \quad (1\text{RSB}) \quad (111)$$

Finally if the phase is FRSB or 1FRSB, then $\chi(q_0) = 1/\sqrt{\Lambda'(q_0)}$ and $\chi(0) = 1/\sqrt{\mu_2}$, leading to

$$J_0^c = \frac{2\gamma + p!}{2\gamma} \sqrt{\frac{pr}{2 + pr}}, \quad (\text{FRSB/1FRSB}) \quad (112)$$

If for a given T , or μ_p , the minimum of J_0 occurs at a physically acceptable finite q_0 with $J_0^* < J_0^c$, then there is a spinodal point and the transition turns discontinuous. Besides the boundary values of q_0 , the minimum of J_0^* may occur at the stationary point of b_p : $db_p/dq_0|_\mu = 0$. A straightforward calculation for the $2 + p$ case yields

$$\begin{aligned} \frac{db_p}{dq_0} \Big|_\mu &= - \frac{1}{(2\gamma + pm^{p-2})^2 \chi(q_0)^2} \\ &\times \left\{ 2\gamma\chi'(q_0) + p[q_0 - (p-1)\chi^2\Lambda(q_0)]\chi'(q_0)m^{p-4} \right. \\ &\quad \left. + \frac{p(p-2)}{2}[1 - \chi^2(q_0)\Lambda'(q_0)]\chi(q_0)m^{p-4} \right\} = 0 \end{aligned} \quad (113)$$

where

$$m^2 = q_0 - \chi(q_0)^2 \Lambda(q_0) \quad (114)$$

In Fig. 5 we report the phase diagram in the (T, J_0) plane for $p = 4$, $r = 0.340$ and $\gamma = 0.8246$. Up to some temperature dependent threshold value

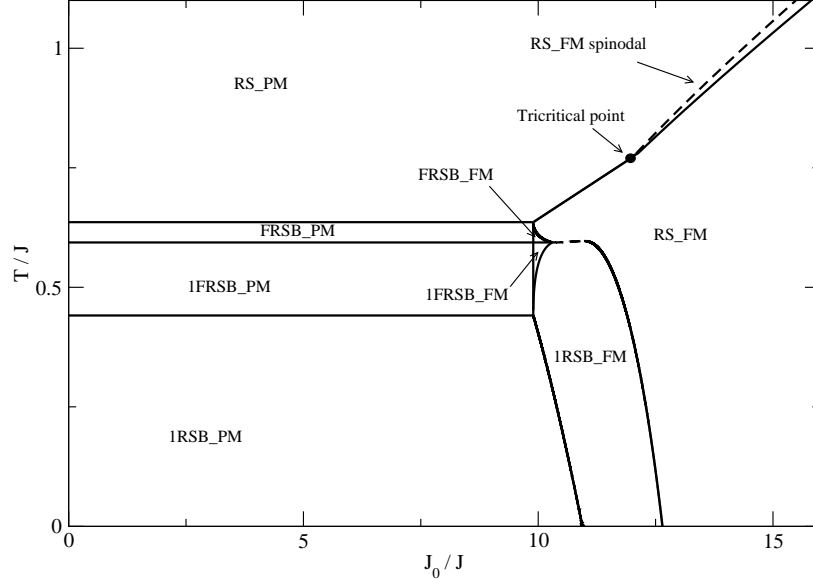


Figure 5: Phase diagram of the 2 + 4 model in the T, J_0 plane for $r = 0.340$ and $\gamma = 0.8246$. The transition between the PM phases ($m = 0$) and the FM phases ($m \neq 0$) is continuous in m up to the tricritical point. Above this point the transition between the paramagnetic phase, denoted RS_PM, and the ferromagnetic phase, denoted RS_FM, is discontinuous with a finite jump of m along the transition line (full line in figure). The transition is accompanied by the appearance of a ferromagnetic spinodal line (dashed line in figure).

of the “ordering parameter” J_0/J , the phases have $m = 0$ (“PM” phases in Figure 5) and are described by the $b = 0$ limit of the solutions discussed in the previous Sections. As J_0/J increases, phases with $m \neq 0$ (FM phases in Figure 5) appear. For low enough temperature the transition between the PM phases and the FM phases occurs continuously with m vanishing at the transition. When the temperature is raised one eventually hits a tricritical point where the transition turns discontinuous. Above this temperature the transition occurs with a finite jump in m on the transition line (full line in Figure 5), and is accompanied by the presence of a spinodal line where the $m \neq 0$ first appears (dashed line). Interestingly, there exists a range of J_0 where, upon cooling, the system goes from a high temperature paramagnetic phase to a low temperature 1RSB spin glass phase with $m = 0$ passing through intermediate FM phases. In this case no continuous transition occurs between the PM and the FM phases. This transition is the counterpart of the 1RSB/RS transition that occurs in the model with a uniform external field.

When $s > 2$ then $b_p \rightarrow \infty$ as $m \rightarrow 0$ and the transition between PM and FM phases can occur only discontinuously with a jump in m .² As an example in Fig.

²A similar scenario also occurs for $2 + p$ models if $\gamma = 0$.

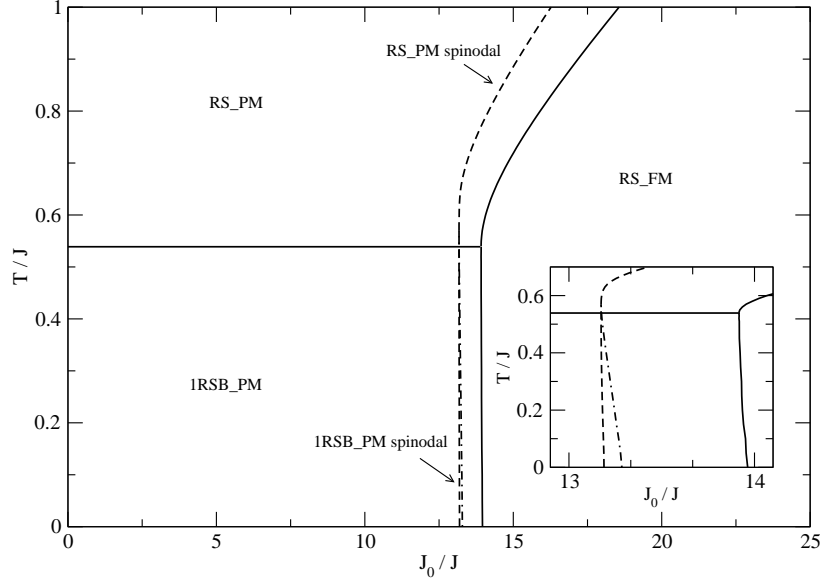


Figure 6: Phase diagram of the $3 + 4$ model in the T, J_0 plane for $r = 0.340$ and $\gamma = 1$. The transition between the PM phases ($m = 0$) and the FM phases ($m \neq 0$) is always discontinuous with a finite jump of m along the transition line (full line in figure). The transition is accompanied by the appearance of a ferromagnetic spinodal line (dashed line in figure). The inset shows the transition line (dash-dotted line) between the (metastable) ferromagnetic 1RSB phase that appears at the spinodal line (dashed line) and the (metastable) ferromagnetic (RS) phase. The latter becomes the thermodynamic stable phase at the transition line (full line on the rhs.).

6 we show the phase diagram of the $3 + 4$ model for $r = 0.75$ and $\gamma = 1$. Note the presence of a phase transition (dash-dotted line) between the (metastable) 1RSB PM solution, which appears at the spinodal line (dashed line), and the (metastable) RS FM solution (see also inset in figure 6).

9. Conclusions

In this work we have studied the spherical multi- p -spin model with ferromagnetic interactions. We formally add multi k -body interaction terms with deterministic interactions next to multi p -body terms with quenched disordered couplings of zero average. A particular case of this set of interactions is to have quenched disorder with non-zero average. After recalling in detail the features of this class of models we have shown that adding purely ferromagnetic terms to the quenched disordered ones can be simply encoded into adding an effective field acting on the purely disordered system. More specifically, once that the presence of the ordered part of the Hamiltonian is encoded into a field, it does not play any role anymore and one can study the systems properties decoupling the analysis of the behavior of a model in a field from the computation of the re-

lationship between the effective field and the real magnetizations brought about by the ferromagnetic couplings. In the replica symmetry breaking parameters, the value of the field only enters in setting the value of the lowest value q_0 of the generic overlap function $q(x)$. This is an increasing function of the field and, hence, the presence of the ferromagnetic contribution can only reduce the “complexity” of the solution found in absence of it. In particular, by increasing the value of the effective field we can eventually force the *frozen* solution to be a RS solution.

We have detailed the analysis of some specific examples whose properties are, though, general. The simplest one is the $3+4$ model, whose phase diagram is akin to a single p -spin model. We then show the behavior of the $2+3$ model, still displaying only RS and 1RSB phases (both with and without ferromagnetic ordering) but whose transitions can be both discontinuous and continuous. On the warm side of the dynamic transition line this is a realization of the mode coupling F_{12} schematic theory [10, 11]. Eventually we exhaustively describe the behavior of the $2+p$ model (with $p \geq 4$) where many phases of different complexity level arise: RS, 1RSB, FRSB and 1FRSB both with and without ferromagnetic ordering. In particular, a continuous breaking of the replica symmetry is realized at low temperature and field in a given region of the phase space, cf. Figs. 2, 5 for the explicit case $p = 4$. From a dynamic perspective the model is equivalent to a mode coupling F_{13} schematic theory [10, 11]. We note that the analysis has been performed using the static approach. When the phase is described by a step-like order parameter function $q(x)$, such as in the 1RSB phase, or it possesses a step-like part, as in the 1FRSB phase, the location of the transition between different phases in the phase space can be different, if one considers the dynamic properties of the system. Roughly speaking this is a consequence of the presence of a macroscopic number of metastable states that prevents the dynamics to reach the lowest (stable) state. The dynamical transition takes place at the point where the metastable states become dominant, and occurs before the static critical point is reached. As far as the phase diagram is concerned the differences between statics and dynamics are then mainly quantitative, not qualitative. In order not to dull reading with too many details we have not explicitly considered this difference in the main text. Nevertheless for completeness a brief technical discussion about dynamic equations and transition lines has been reported in Appendix B.

Acknowledgments

The authors acknowledge F. Krzakala, Y.F. Sun, and L. Zdeborova for stimulating interaction. The research leading to these results has received funding from the People Programme (Marie Curie Actions) of the European Union’s Seventh Framework Programme FP7/2007-2013/ under REA grant agreement n 290038, NETADIS project and from the Italian MIUR under the Basic Research Investigation Fund FIRB2008 program, grant No. RBFR08M3P4, and under the PRIN2010 program, grant code 2010HXAW77-008.

Appendix A. 1RSB-1FRSB critical surface for the $2 + p$ model

The 1RSB equations for the $2 + p$ model are

$$\mu_2 q_0 + \mu_p q_0^{p-1} = \frac{q_0}{\chi(q_0)^2} - b^2 \quad (\text{A.1})$$

$$\mu_2(q_1 - q_0) + \mu_p(q_1^{p-1} - q_0^{p-1}) = \frac{q_1 - q_0}{\chi(q_1)\chi(q_0)} \quad (\text{A.2})$$

where

$$\chi(q_1) = 1 - q_1, \quad \chi(q_0) = 1 - q_1 + x(q_1 - q_0) \quad (\text{A.3})$$

and the breaking point x is fixed by equation (53). The 1RSB phase is stable provided the eigenvalue $\Lambda_0^{(3)}$, eq. (57), is positive. This leads to the critical condition

$$\Lambda'(q_0) = \frac{1}{\chi(q_0)^2} \Rightarrow \mu_2 + \mu_p(p-1)q_0^{p-2} = \frac{1}{\chi(q_0)^2}. \quad (\text{A.4})$$

By introducing the ratio $t = q_0/q_1 \in [0, 1]$, and solving the equations for μ_2 and μ_p , we obtain the equation of the 1RSB critical line

$$\mu_p = \frac{1}{x^2 y (1-y)^{p-3} (1-t)} \frac{[1-y+xy(1-t)]^p}{[1-(p-1)t^{p-2}+(p-2)t^{p-1}]} \quad (\text{A.5})$$

$$\mu_2 = \frac{[y(1-t^{p-1})-(p-1)(1-t)t^{p-2}]}{x^2 y (1-t)^2} \quad (\text{A.6})$$

$$b^2 = (p-2) \frac{t^{p-1}(1-y)^2}{x^2 y (1-t)} \frac{[1-y+xy(1-t)]}{[1-(p-1)t^{p-2}+(p-1)t^{p-1}]} \times \frac{[1-y+xy(1-t)]^2}{[1-(p-1)t^{p-2}+(p-2)t^{p-1}]} \quad (\text{A.7})$$

where y and t are related by the equation

$$z(y) = \left\{ y[p-2-pt+pt^{p-1}-(p-2)t^p] + 2 - p(p-1)t^{p-2} + 2p(p-2)t^{p-1} - (p-1)(p-2)t^p \right\} \times \frac{1}{p(1-t)[1-(p-1)t^{p-2}+(p-2)t^{p-1}]} \quad (\text{A.8})$$

and

$$r = \frac{\mu_2}{\mu_p} = \frac{(1-y)^{p-3}}{(1-t)} \frac{[y(1-t^{p-1})-(p-1)t^{p-2}]}{[1-y+xy(1-t)]^{p-2}}. \quad (\text{A.9})$$

For the 2 + 4 spherical model the equations can be simplified as follows

$$\mu_4 = \frac{[1 - y + xy(1 - t)]^4}{(1 - t)^3(1 + 2t)x^2y(1 - y)} \quad (\text{A.10})$$

$$\mu_2 = \frac{[y(1 + t + t^2) - 3t^2][1 - y + xy(1 - t)]^2}{(1 - t)^3(1 + 2t)x^2y} \quad (\text{A.11})$$

$$b^2 = 2 \frac{t^3(1 - y)^2[1 - y + xy(1 - t)]}{(1 - t)^3(1 + 2t)x^2y}, \quad (\text{A.12})$$

where y is solution of

$$z(y) = \frac{1 + 3t + y(1 + t)}{2(1 + 2t)}, \quad (\text{A.13})$$

and

$$r = \frac{\mu_2}{\mu_4} = (1 - y) \frac{y(1 + t + t^2) - 3t^2}{[1 - y + xy(1 - t)]^2}. \quad (\text{A.14})$$

Equation (A.8), or (A.13) for the 2 + 4 case, can be solved by fixing the value of either y or t in the range $[0, 1]$, and solving for the other. Once x , y and t are known, μ_p , μ_2 and b are obtained from eqs. (A.5), (A.6) and (A.7). The other quantities are given by

$$q_1 = \frac{1 - y}{1 - y + xy(1 - t)}, \quad \chi(q_0) = \frac{x(1 - t)}{1 - y + xy(1 - t)} \quad (\text{A.15})$$

with $q_0 = tq_1$, $\chi(q_1) = y\chi(q_0)$.

By fixing x and solving for y as function of t one finds the x -lines in the (μ_p, μ_2, b) space along which the 1RSB phase becomes unstable. These are obtained by setting $t = 0$ ($q_0 = 0$) into Eqs. (A.5), (A.6) and (A.8), and are reported in Sec. 7, cf. Eqs. (86)-(88).

In Sec. 7 we also report the boundary values $r_x^{(t)}$ for which the constant r (μ_4, b) projections start displaying different phases, cf. Eqs. (84), (90), (91), (96).

The 1RSB-1FRSB critical surface ends when $t = 1$ where the discontinuity associated with the 1RSB (and 1FRSB) solution disappears. Solving equation (A.8) in the limit $t \rightarrow 1^-$ we obtain

$$y = 1 - \frac{p - 3}{3}(1 - t) + O((1 - t)^2), \quad t \rightarrow 1^- \quad (\text{A.16})$$

and

$$q_1 = \frac{p - 3}{p - 3(1 - x)} + O(1 - t), \quad q_1 - q_0 = O(1 - t), \quad t \rightarrow 1^-. \quad (\text{A.17})$$

The equation of the critical end line of the 1RSB-1FRSB critical surface are reported in Sec. 7, cf. Eqs. (92)-(94).

Appendix B. Dynamic transition

When the solution is described by a step-like order parameter function $q(x)$, such as in the 1RSB phase, or it possesses a step-like part, as in the 1FRSB phase, the location of the transition between different phases in the phase space can be different, depending one considers the static or dynamic properties of the system. This is a consequence of the appearance of a macroscopic number of metastable states that prevents the dynamics to reach the lowest (stable) state [49, 50, 51, 52]. In this case the dynamical evolution of the system is dominated by these metastable states and the system fails to reach the static critical point. The dynamical transition is associated with the point where the effect of the metastable states becomes dominant, and occurs before the static critical point is reached.

We do not go into the details of a dynamical study of the model, but rather use a shortcut that allows us to recover the dynamical properties from the replica calculation described in the main text. This accounts for replacing the stationary condition of the free energy functional $G[q, m]$ with respect to variations of the breaking point x (or x_1 for the 1FRSB solution) by the (simpler) “marginal condition”

$$\Lambda_1^{(1)} = -\Lambda'(q_1) + \frac{1}{\chi(q_1)^2} = 0 \quad (\text{B.1})$$

which describes the critical slowing down of the dynamics at the dynamic transition point. The interested reader can find more details on this in, e.g., Ref. [38]. Once this replacement has been done, the study of the phase diagram just follows the same mainlines of described in the main text for the static solution.

For example by solving eqs. (49) and (B.1) we have for the 1RSB phase of the $s + p$ model the parametric equations:

$$\mu_s = \frac{1}{\chi_1^2 \chi_0} \frac{(q_1^{p-1} - q_0^{p-1})\chi_0 - (p-1)q_1^{p-2}(q_1 - q_0)\chi_1}{(s-1)q_1^{s-2}(q_1^{p-1} - q_0^{p-1}) - (p-1)q_1^{p-2}(q_1^{s-1} - q_0^{s-1})} \quad (\text{B.2})$$

$$\mu_p = \frac{1}{\chi_1^2 \chi_0} \frac{(q_1^{s-1} - q_0^{s-1})\chi_0 - (s-1)q_1^{s-2}(q_1 - q_0)\chi_1}{(p-1)q_1^{p-2}(q_1^{s-1} - q_0^{s-1}) - (s-1)q_1^{s-2}(q_1^{p-1} - q_0^{p-1})} \quad (\text{B.3})$$

where $\chi_{0,1} = \chi(q_{0,1})$, which give (μ_s, μ_p) as function of (q_0, q_1, x) . These equations, with b obtained from eq. (48), give the complete description of the 1RSB solution in the dynamic approach.

In the limit $q_1 - q_0 \rightarrow 0$ the stationary condition used in statics and the marginal condition used in dynamics coincide, so that all “continuous transition” are unchanged between static and dynamics. This is not true for the discontinuous transition where $q_1 - q_0$ remains finite. To obtain the discontinuous transition surface between the RS and 1RSB phase, we take $x = 1$ in the above equations and vary q_1 and q_0 . This surface is qualitatively similar to the analogous surface discussed for the static, and, indeed, it joins the continuous transition surface along the same line discussed in the main text, but it is

everywhere else distinct from that. It crosses the $b = 0$ plane along the line

$$\mu_s = \frac{p-2-(p-1)q_1}{(p-s)q_1^{s-2}(1-q_1)^2} \quad (\text{B.4})$$

$$\mu_p = \frac{(s-1)q_1-(s-2)}{(p-s)q_1^{p-2}(1-q_1)^2} \quad (\text{B.5})$$

which lies on the left hand side of the corresponding static line in the (μ_p, μ_s) plane.

The critical surface between the 1RSB and the 1FRSB phases of the $2+p$ model is obtained from the above equations by imposing the additional critical condition (A.4), which reduces the number of free parameters from 3 to 2. A straightforward calculations leads again to eqs. (A.5)-(A.7) with

$$y = \frac{1-(p-1)t^{p-2}+(p-2)t^{p-1}}{(p-1)(1-t)-(1-t^{p-1})} \quad (\text{B.6})$$

replacing eq. (A.8). This surface intersects the continuous 1RSB-RS transition surface along the same line discussed in the main text for the static, eqs. (92)-(94), and the $b = 0$ plane on the line of equation (86)-(87) with $y_0 = 1/(p-2)$. The analysis for other cases is straightforward.

References

References

- [1] T. H. Berlin, M. Kac, *The spherical model of a ferromagnet*, Phys. Rev. **86** (1952) 821835.
- [2] T. Kirkpatrick, D. Thirumalai, *p-spin-interaction spin-glass models: Connections with the structural glass problem*, Phys. Rev. B **36** (1987) 5388.
- [3] T. Kirkpatrick, D. Thirumalai, *Dynamics of the structural glass transition and the p-spin interaction spin-glass model*, Phys. Rev. Lett. **58** (1987) 2091.
- [4] D. Thirumalai, T. Kirkpatrick, *Mean-field Potts glass model: Initial-condition effects on dynamics and properties of metastable states*, Phys. Rev. B **38** (1988) 4881.
- [5] A. Crisanti, H. Sommers, *The spherical p-spin interaction spin-glass model - the statics*, Z. Phys. B **87** (1992) 341.
- [6] A. Crisanti, L. Leuzzi, *Amorphous-amorphous transition and the two-step replica symmetry breaking phase*, Phys. Rev. B **76** (2007) 184417.
- [7] A. Crisanti, L. Leuzzi, M. Paoluzzi, *Statistical mechanical approach to secondary processes and structural relaxation in glasses and glass formers*, Eur. Phys. J. E **34** (2011) 98.

- [8] M. Romanini, P. Negrier, J. L. Tamarit, S. Capaccioli, M. Barrio, L. C. Pardo, D. Mondieig, *Emergence of glassy-like dynamics in an orientationally ordered phase*, Phys. Rev. B **85** (2012) 134201.
- [9] K. L. Ngai, *Relaxation and Diffusion in Complex Systems*, Springer Verlag (New York), 2011.
- [10] W. Götze, L. Sjögren, *Beta relaxation near glass transition singularities*, J. Phys.: Cond. Matt. **1** (1989) 4183.
- [11] W. Götze, L. Sjögren, *Logarithmic decay laws in glassy systems*, J. Phys.: Cond. Matt. **1** (1989) 4203.
- [12] W. Götze, *Complex Dynamics of Glass-Forming Liquids: A Mode-Coupling Theory*, OUP (Oxford, UK), 2009.
- [13] M. Mézard, G. Parisi, *Replica field theory for random manifolds*, J. Phys. I **1** (1991) 809.
- [14] T. Giamarchi, P. Le Doussal, *Elastic theory of pinned flux lattices*, Phys. Rev. Lett. **72** (1994) 1530.
- [15] T. Giamarchi, P. Le Doussal, *Elastic theory of flux lattices in the presence of weak disorder*, Phys. Rev. B **52** (1995) 1242.
- [16] L. F. Cugliandolo, J. Kurchan, P. Le Doussal, *Large Time Out-of-Equilibrium Dynamics of a Manifold in a Random Potential*, Phys. Rev. Lett. **76** (1996) 2390.
- [17] P. Le Doussal, K. J. Wiese, *Glassy Trapping of Manifolds in Nonpotential Random Flows*, Phys. Rev. Lett. **80** (1998) 2362.
- [18] T. Nieuwenhuizen, *To maximize or not to maximize the free energy of glassy systems*, Phys. Rev. Lett. **74** (1995) 3463.
- [19] A. Crisanti, L. Leuzzi, *Spherical $2+p$ spin-glass model: An exactly solvable model for glass to spin-glass transition*, Phys. Rev. Lett. **93** (2004) 217203.
- [20] A. Crisanti, L. Leuzzi, *Spherical $2+p$ spin-glass model: An analytically solvable model with a glass-to-glass transition*, Phys. Rev. B **73** (2006) 014412.
- [21] D. Sherrington, S. Kirkpatrick, *Solvable Model of a Spin-Glass*, Phys. Rev. Lett. **35** (1975) 1792.
- [22] H. Nishimori, *Statistical Physics of Spin Glasses and Information Processing: An Introduction*, Oxford University Press (Oxford), 2001.
- [23] F. Krzakala, L. Zdeborová, *On melting dynamics and the glass transition. II. Glassy dynamics as a melting process*, J. Chem. Phys. **134** (2011) 034513.

- [24] A. Barrat, S. Franz, G. Parisi, *Temperature evolution and bifurcations of metastable states in mean-field spin glasses, with connections with structural glasses*, J. Phys. A: Math. Gen. **30** (1997) 5593.
- [25] B. Capone, T. Castellani, I. Giardina, F. Ricci-Tersenghi, *Off-equilibrium confined dynamics in a glassy system with level-crossing states*, Phys. Rev. B **74** (2006) 144301.
- [26] Y. F. Sun, A. Crisanti, F. Krzakala, L. Leuzzi, L. Zdeborov, *Following states in temperature in the spherical $s + p$ -spin glass model*, J. Stat. Mech. (2012) P07002.
- [27] F. Thalmann, C. Dasgupta, D. Feinberg, *Phase diagram of a classical fluid in a quenched random potential*, Europhys. Lett. **50** (2000) 5460.
- [28] V. Krakoviack, *Mode-coupling theory for the slow collective dynamics of fluids adsorbed in disordered porous media*, Phys Rev E **75** (2007) 031503.
- [29] V. Krakoviack, *Statistical mechanics of homogeneous partly pinned fluid systems*, Phys Rev E **82** (2010) 061501.
- [30] A. Gordon, B. Fischer, *Phase Transition Theory of Many-Mode Ordering and Pulse Formation in Lasers*, Phys. Rev. Lett. **89** (2002) 103901.
- [31] A. Gordon, B. Fischer, *Phase transition theory of pulse formation in passively mode-locked lasers with dispersion and Kerr nonlinearity*, Opt. Comm. **223** (2003) 151–156.
- [32] R. Weill, A. Rosen, A. Gordon, O. Gat, B. Fischer, *Critical Behavior of Light in Mode-Locked Lasers*, Phys. Rev. Lett. **95** (1) (2005) 013903.
- [33] H. Cao, Y. G. Zhao, S. T. Ho, E. W. Seelig, Q. H. Wang, R. P. H. Chang, *Random Laser Action in Semiconductor Powder*, Phys. Rev. Lett. **82** (1999) 2278.
- [34] D. S. Wiersma, *The physics and applications of random lasers*, Nature Physics **4** (2008) 359.
- [35] L. Leuzzi, C. Conti, V. Folli, L. Angelani, G. Ruocco, *Phase Diagram and Complexity of Mode-Locked Lasers: From Order to Disorder*, Phys. Rev. Lett. **102** (2009) 083901.
- [36] C. Conti, L. Leuzzi, *Complexity of waves in nonlinear disordered media*, Phys. Rev. B **83** (2011) 134204.
- [37] A. Crisanti, H. Horner, H. Sommers, *The spherical p -spin interaction spin-glass model - the dynamics*, Z. Phys. B **92** (1993) 257.
- [38] A. Crisanti, L. Leuzzi, *Equilibrium Dynamics of Spin-Glass Systems*, Phys. Rev. B **75** (2007) 144301.

- [39] J. Hertz, D. Sherrington, T. Nieuwenhuizen, *Competition between glassiness and order in a multispin glass*, Phys. Rev. E **60** (1999) R2460–3.
- [40] V. Krakoviack, Comment on “spherical $2 + p$ spin-glass model: An analytically solvable model with a glass-to-glass transition”, Phys. Rev. B **76** (2007) 136401.
- [41] A. Crisanti, L. Leuzzi, Reply to “comment on ‘spherical $2 + p$ spin-glass model: An analytically solvable model with a glass-to-glass transition’ ”, Phys. Rev. B **76** (2007) 136402.
- [42] M. Mézard, G. Parisi, M. Virasoro, *Spin Glass Theory and Beyond*, World Scientific (Singapore), 1987.
- [43] G. Parisi, *Infinite Number of Order Parameters for Spin-Glasses*, Phys. Rev. Lett. **43** (1979) 17541756.
- [44] G. Parisi, *Toward a mean field theory for spin glasses*, Phys. Lett. A **73** (1979) 203–205.
- [45] G. Parisi, *A sequence of approximated solutiona to the S-K model for spin glasses*, J. Phys. A: Math. Gen. **13** (1980) L115.
- [46] D. M. Carlucci, C. De Dominicis, T. Temesvari, *Stability of the Mzard-Parisi Solution for Random Manifolds*, J. Phys. I (France) **6** (1996) 1031.
- [47] C. De Dominicis, D. M. Carlucci, T. Temesvari, *Replica Fourier Tansforms on Ultrametric Trees, and Block-Diagonalizing Multi-Replica Matrices*, J. Phys. I (France) **7** (1997) 105–115.
- [48] A. Crisanti, F. Ritort, *Intermittency of glassy relaxation and the emergence of a non-equilibrium spontaneous measure in the aging regime*, Europhys. Lett. **66** (2004) 253.
- [49] A. Crisanti, H. Sommers, *Thouless-Anderson-Palmer approach to the spherical p -spin spin glass model*, J. Phys. I (France) **5** (1995) 805–813.
- [50] A. Cavagna, I. Giardina, G. Parisi, *Stationary points of the Thouless-Anderson-Palmer free energy*, Phys. Rev. B **57** (1998) 11251.
- [51] A. Cavagna, J. P. Garrahan, I. Giardina, *Quenched complexity of the mean-field p -spin spherical model with external magnetic field*, J. Phys. A **32** (1998) 711.
- [52] A. Crisanti, L. Leuzzi, T. Rizzo, *The Complexity of the Spherical p -spin spin glass model, revisited*, Eur. Phys. J. B **36** (2003) 129–136.